INORGANIC CHEMISTRY
FRONTIERS

RESEARCH ARTICLE

View Article Online
View Journal

Cite this: DOI: 10.1039/d6qi00446f

Biphasic modulation of Aβ(1–40) self-assembly by porphyrins: effects of concentration and structural variation

Adèle Brison, Geneviève Pratviel and Christelle Hureau *

Aβ peptides self-assemble into senile plaques, a hallmark of Alzheimer's disease (AD). The search for compounds able to modulate peptide self-assembly still awaits molecular and structural insights. In the present work, we have investigated a series of cationic porphyrins. By monitoring the kinetics of peptide self-assembly using thioflavin T (ThT) fluorescence and imaging the formed assemblies by TEM and AFM, we observed the following: (i) first, some porphyrins accelerate Aβ(1–40) self-assembly to an extent that increases with the porphyrin concentration. For the others, a decrease in the kinetic rates was observed above a concentration threshold (denoted as C_M) that is porphyrin-dependent. The biphasic modulation thus observed has not been reported so far in the case of porphyrins; (ii) second, the porphyrins decrease the level of Aβ(1–40) fibrils formed as their concentration increases. The interactions between the porphyrins and Aβ(1–40) were thoroughly characterized by UV-visible, NMR, and fluorescence spectroscopy techniques. The obtained data support a structure-dependent model involving π-stacking, electrostatic and hydrophobic interactions responsible for the different effects of porphyrins on Aβ(1–40) self-assembly.

Received 6th March 2026,
Accepted 7th May 2026

DOI: 10.1039/d6qi00446f

rsc.li/frontiers-inorganic

Introduction

Amyloid-related diseases, such as Alzheimer's disease (AD), Parkinson's disease, and type II diabetes, all rely on a common mechanism involving the self-assembly of a disease-specific intrinsically disordered peptide.[1–5] In the case of AD, the peptide involved is amyloid-β (Aβ). Its overproduction and accumulation as aggregates and fibrils in senile plaques are among the hallmarks of AD. Aβ self-assembly is currently regarded as a major contributor to the neuronal damage and memory impairment observed in the AD brain.[6–10]

Aβ is a 40–42 amino acid residue peptide built on three main domains: (i) the N-terminal part rich in histidine (His) and carboxylate-containing residues and where metal ions can bind,[11,12] (ii) the regions involved in β-strand formation that gather the central hydrophobic core (CHC) and the C-terminal part of the peptide, and (iii) the residues involved in the formation of a turn (Scheme 1A).[13,14] At pH 7.4, the Aβ peptide is anionic, with a charge of about −2.7.

The process by which Aβ peptides self-assemble is highly intricate, and several species, such as soluble oligomers, amorphous aggregates and proto-fibrils, are formed prior to and/or in parallel with the thermodynamically stable, β-sheet-rich fibrils.[11,15,16] Briefly, self-assembly proceeds *via* nucleation–elongation supramolecular polymerization. It relies on the formation of nuclei that can further elongate at their extremities. In addition, the pool of nuclei can be fueled by secondary nucleation processes, mainly fragmentation and fibril-catalyzed nucleation (Scheme 1B).[17–23] Association of several fibrils can also occur and lead to the formation of twisted assemblies.

Inhibition of Aβ self-assembly is considered a therapeutic approach of interest that can be achieved by employing well-designed molecules,[24–32] beyond immunotherapy.[7–10] Such molecules are aromatic-rich and/or charged compounds able to interact with the aromatic, hydrophobic, charged residues and/or metal-binding residues of the Aβ peptide. As a general trend, their mode of action relies on the stabilization of Aβ peptides in their monomeric form, thus preventing self-association. Porphyrins have been studied as modulators of the self-assembly of several amyloid-forming peptides, including the Aβ peptide;[33–36] the Tau protein involved in AD;[37] α-synuclein involved in Parkinson's disease;[38–41] and insulin[42,43] and amylin,[44–46] both of which are involved in type II diabetes.

With respect to Aβ, it has been reported that the stoichiometric ratio of the cationic porphyrin *meso*-5,10,15,20-tetrakis (*N*-methylpyridinium-4-yl) porphyrin, **H_2-TMPyP**, inhibits the formation of Aβ(1–42) oligomers and fibrils, induces the dismantling of preformed Aβ aggregates and alleviates Aβ(1–42)-

Univ Toulouse, CNRS, LCC, Toulouse, France.
E-mail: christelle.hureau@lcc-toulouse.fr

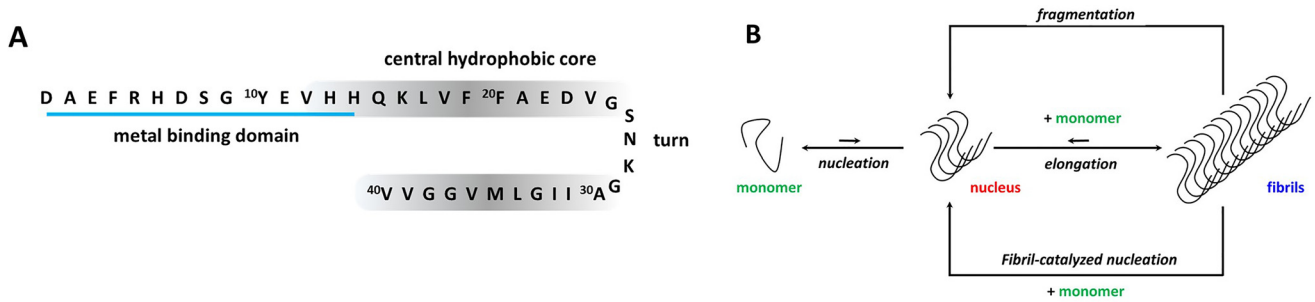

Scheme 1 (A) Sequence of the Aβ(1–40) peptide and regions of interest. (B) Self-assembly process of the Aβ peptide.

induced cytotoxicity in neuroblastoma SH-SY5Y cells.[33] A neutral porphyrin was very recently reported to have a moderate effect on Aβ self-assembly.[47] Finally, the anionic porphyrin, *meso*-5,10,15,20-tetrakis(4-sulfonatophenyl)porphyrin, **H_2-TPPS**, does not influence Aβ(1–42) aggregation,[34] although it has some impact on the cationic amylin peptide.[45]

The most typical and characterized example of a metalloporphyrin interacting with the Aβ peptide is heme (iron(III)-protoporphyrin IX), which has been found to co-localize with Aβ in senile plaques in post-mortem AD brains, and thus, it has attracted much attention. Heme was shown early on to modulate Aβ aggregation.[35,36,48] The best-characterized interaction of heme with Aβ peptides is its coordination with the His residues in a way reminiscent of the heme binding in peroxidase enzymes.[48–51] Zn-porphyrins that can also interact with Aβ His residues have been shown to impact Aβ aggregation as well.[52,53]

In the present work, we aim at enlarging the family of porphyrins capable of interacting with Aβ and modulating its self-assembly propensity. Our goal is to establish a structure–activity relationship (SAR) and provide deeper insights into their modes of action. Hence, we studied the effects of a series of cationic porphyrins on the kinetics of Aβ(1–40) self-assembly and on the morphology of the formed fibrils using a combination of spectroscopic and microscopic imaging methods. We used Aβ(1–40) because it exhibits more moderate and reproducible self-assembly behaviour than Aβ(1–42).[54,55] The porphyrin series includes the commercially available **H_2-TMPyP** and the still-unexplored **H_2-MA**, another cationic porphyrin with longer arms. One negatively charged porphyrin (**H_2-TPPS**) is used for comparison purposes. We have also studied the influence of the insertion of two metal cations (Au(III) and Cu(II)) in the center of the cationic porphyrins. In addition, we have probed the effect of porphyrin concentration (*id est*, the porphyrin/Aβ(1–40) ratio), a parameter that has not been explored so far. Our data indicate that the TMPyP family interacts with the Aβ(1–40) peptide, leading to an acceleration of peptide self-assembly and that the **MA** family induces a biphasic effect. In the latter case, the acceleration is maximal at a given porphyrin concentration that is dependent on the exact nature of the porphyrin. For all the cationic porphyrins studied, the prevention of fibril formation was observed and increased with the porphyrin concentration. The deduced SAR shows that (i) interactions between the porphyrins and the Aβ peptide are mainly governed by electrostatic and π-stacking forces, while the size of the porphyrin also matters; (ii) two sites of interaction coexist; and (iii) the stronger the interactions of the porphyrins with the first site are, the higher the increase in the self-assembly rate is.

Experimental section

Chemicals and reagents

All solutions were prepared using ultrapure water. HEPES buffer (2-[4-(2-hydroxyethyl)piperazin-1-yl]ethanesulfonic acid sodium salt) and ethylenediaminetetraacetic acid (EDTA) were bought from Sigma-Aldrich. ThioflavinT (ThT) was bought from Acros Organics. The anionic porphyrin *meso*-tetra(4-sulfonatophenyl)porphyrin dihydrochloride (**H_2-TPPS**) was purchased from Frontier Scientific. Cationic porphyrins were prepared as previously reported (**H_2-TMPyP** and **H_2-MA**,[56] **Au-MA**[57] and **Cu-MA**[58]). Stock solutions of porphyrins (1 mM) and ThT (250 μM) in water were stored at −20 °C. Aβ(1–40) (sequence: DAEFRHDSGYEVHHQKLVFFAEDVGSNKGAIIGLMVGGVV) was purchased from GeneCust (Dudelange, Luxembourg) with a purity grade >95%. It was purified by FPLC (fast protein liquid chromatography; size exclusion) according to previously reported protocols,[59,60] to obtain a monomeric fraction of Aβ(1–40) prior to use in self-assembly experiments. The peptide concentration was measured by UV-vis absorption of tyrosine (one residue per peptide, Tyr10) at basic pH ($\varepsilon_{293-360}$ = 2400 M^{-1} cm^{-1}).[61]

Kinetic measurements of Aβ(1–40) self-assembly by ThT and porphyrin fluorescence

Fluorescence experiments were performed using a BMG LABTECH FLUOstar OPTIMA at 37 °C with black 384-well plates (Greiner Bio-One). ThT was excited at 440 nm, and the fluorescence emission was recorded at 490 nm. The gain was 1400. Fluorescence was measured at fixed intervals of 10 min preceded by a given period of stirring (15 s at 200 rpm in double-orbital mode). Samples were prepared by mixing appro-

priate volumes of stock solutions of 500 mM HEPES buffer pH 7.4 (containing 100 nM EDTA), 1 mM porphyrin in water, 250 μM ThT in water and 40 μM Aβ(1–40) peptide in water and about 20% FPLC eluant (NaCl 150 mM, NaOH 15 mM). The final concentrations were as follows: 100 mM HEPES buffer, 20 nM EDTA, 1 to 40 μM porphyrin (see text or figures' captions), 20 μM Aβ(1–40) peptide and 10 μM ThT in a final volume of 50 μL per well. In addition to the measurement of ThT fluorescence during the process of peptide self-assembly, the fluorescence of selected porphyrins was also monitored (excitation at 410 nm and emission at 640 nm, using dedicated filters) every 10 min with a gain value between 1400 and 2700.

Evaluation of the kinetic parameters of Aβ assembly

The ThT fluorescence increase can be considered, in general, by a sigmoidal curve according to the following equation:

$$F(t) = F_0 + \frac{F_{\max} - F_0}{1 + e^{-k(t-t_{1/2})}} = F_0 + \frac{\Delta F}{1 + e^{-k(t-t_{1/2})}}$$

where F_0 is the initial ThT fluorescence value, ΔF is the ThT fluorescence increase ($F_{\max} - F_0$), k is the growth rate, and $t_{1/2}$ is the time at which the ThT fluorescence increase equals half of its maximal value. To compare all curves, a custom routine was developed to straightforwardly evaluate the key parameters.[60] ThT curves were first normalized. The inflection point, $t_{1/2}$ was determined as the time at which $F(t) = F_0 + \frac{\Delta F}{2}$. An apparent growth rate, later noted for the matter of simplicity as $k_{t_{1/2}}$, was estimated by calculating the slope at $t = t_{1/2}$ as $k = 4\left(\frac{F_{60\%} - F_{40\%}}{t_{60\%} - t_{40\%}}\right)$, where $F_{60\%}$ and $F_{40\%}$ equal 60% and 40% of the maximal ThT fluorescence increase, respectively, and $t_{60\%}$ and $t_{40\%}$ are the times at which these fluorescence values occur. The $\frac{1}{4}$ factor arises from the fact that the slope at the inflection point ($t = t_{1/2}$) for a sigmoidal equation $S(t) = \frac{1}{1 + e^{-k(t-t_{1/2})}}$ is equal to $S'(t_{1/2}) = \frac{k}{4}$.

The self-assembly of Aβ(1–40) was studied using several different batches to ensure that the effects seen were not batch-dependent. At least 2 independent experiments with 6 replicates for each condition were performed. Data from one experiment are shown in the full text, while additional data can be found in the SI. To compare the parameters from one experiment to another, normalization with respect to the Aβ(1–40) self-assembly in the absence of porphyrins (from the very same experiment) was performed by dividing the measured mean value of a given parameter by the mean value of the same parameter obtained for Aβ(1–40) alone.

Transmission electron microscopy (TEM)

After 3 days of self-assembly in 384-well plates (see the previous paragraph for details), samples were prepared for electron microscopy by using a conventional negative-staining procedure. An aliquot (10 μL) of each sample was adsorbed onto Formvar-carbon-coated grids for 1 min, blotted, and negatively stained with uranyl acetate (1%) for 1 min. The grids were examined using a TEM (Jeol JEM-1400, JEOL Inc., Peabody, MA, USA) at 80 kV. Images were acquired by using a digital camera (Gatan Orius, Gatan Inc., Pleasanton, CA, USA) at different magnifications: 3000 (2 μm scale), 6000 (1 μm scale), 12 000 (0.5 μm scale), and 20 000 (100 nm scale).

Atomic force microscopy (AFM)

After 3 days of self-assembly in 384-well plates (see the previous paragraph for details), samples were prepared for atomic force microscopy by using a conventional procedure.[62] Briefly, a drop of sample (10 μL) was deposited onto freshly cleaved mica and left for 1 h to adsorb onto the substrate. It was then washed with deionized water (50 μL) to remove the salt and dried with pressurized air before imaging. The AFM pictures were captured in air using a Smart SPM-1000 microscope (AIST-NT, Novato, USA) equipped with a 100 μM scanner. Si cantilevers (NanoWorld, Switzerland) with an elastic modulus of ≈42 N m^{-1} were used. All images were recorded as 512 × 512 pixel images at a typical scan rate of 0.2 kHz with a vertical tip oscillation frequency of 250–350 kHz. Representative images of each sample were obtained by scanning at least 3 different locations.

UV-visible measurements

Spectra were recorded on a CLARIOstar spectrometer in 384 plaques under the very same conditions as the ThT experiments at the beginning and the end of the self-assembly process. Porphyrins were added to 100 mM HEPES buffer, pH 7.4, 20 nM of EDTA in the absence of peptide or in the presence of 20 μM Aβ(1–40) at 37 °C.

^{1}H-1D NMR

All spectra were recorded on a Bruker Ascend 600 spectrometer equipped with a 5 mm triple-resonance inverse Z-gradient probe (TBI ^{1}H, ^{31}P, BB). Chemical shifts for ^{1}H were relative to TMS (tetramethylsilane) using the ^{1}H (residual) chemical shifts of the solvent as a secondary standard. The peptide concentration was 200 μM in 10 mM HEPES-d_{18} buffer, pH 7.4, 10% D_2O. Porphyrins were dissolved in H_2O at 1 mM concentration, and appropriate aliquots were added to the test tube so that the final molar ratio varied from 1% to 20% of porphyrin. The ^{1}H NMR spectra were acquired at 298 K using the Bruker pulse program 'zgesp,' featuring a water-suppression sequence and the following parameters: spectral width, 12 ppm; 30° nutation angle duration, 9.5 μs; and recycling delay, 2 s (1 s acquisition time and 1 s relaxation delay).

Results and discussion

The porphyrins used in the present study are shown in Scheme 2. They are charged and thus soluble in water. The non-metallated porphyrin scaffold bears four charges, located at different positions on the *meso*-substituents. Our study introduces **H_2-MA**, a novel porphyrin that has not been investi-

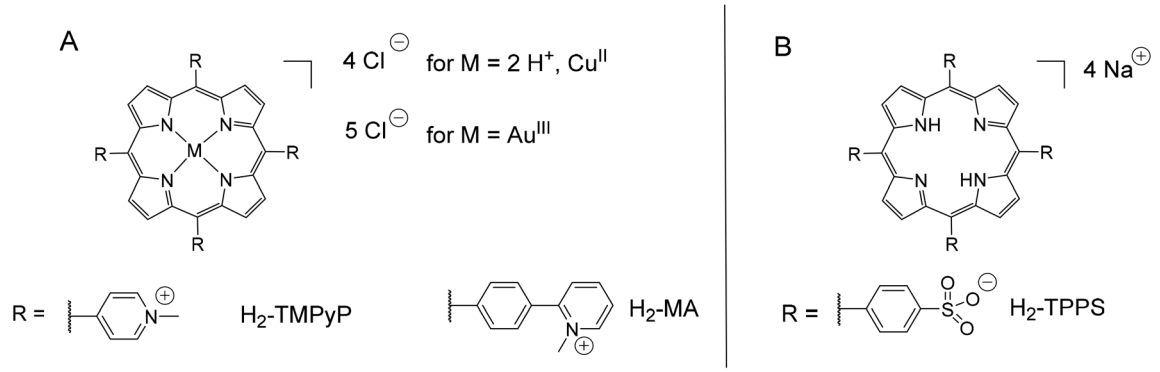

Scheme 2 (A) Structures of the cationic porphyrins; M = $2H^+$ denotes the non-metalled porphyrins. (B) Structure of the anionic porphyrin.

gated in the context of amyloid formation. Structurally, **H_2-MA** features four identical arms and is derived from the commercially available and previously studied **H_2-TMPyP** (Scheme 2A) and has been originally synthesized for interacting with the minor groove of DNA.[56,63] **H_2-MA** was chosen to explore the influence of arm length and aromatic interactions while maintaining the same charge as **H_2-TMPyP**. The extended aromatic system in **H_2-MA** enhances π-stacking interactions and electron delocalization, potentially amplifying its effect on Aβ self-assembly. Its positive charges are farther from the tetrapyrrole scaffold compared to the reference **H_2-TMPyP** since the *meso*-substituents are bulkier than the pyridinium groups of **H_2-TMPyP**. Furthermore, the electron richness of the porphyrin core is higher than that of **H_2-TMPyP** due to the remoteness of the pyridinium groups. The Au(III) counterparts of **H_2-TMPyP** and **H_2-MA** as well as **Cu(II)-MA** were also included in the study. While Fe-,[36,38,39,45,46,64] Zn-,[34,47,53] and Mn-porphyrins[34,46,64,65] have been studied in the context of amyloid-forming peptide self-assembly, Cu-[34,43] and Au-porphyrins have received less attention in the literature. This highlights an opportunity for further exploration of these metalloporphyrins in modulating Aβ self-assembly.

The commercially available anionic porphyrin, **H_2-TPPS**, bearing four negative charges, was included in the series of the tested compounds for comparison purposes (Scheme 2B).

Influence of the porphyrins on the fibrillation of the Aβ(1–40) peptide

The self-assembly of Aβ(1–40) was monitored by a standard approach using thioflavin T (ThT)[66,67] fluorescence and TEM and AFM imaging at the end of the self-assembly. 2 to 4 independent experiments were performed for each porphyrin (see Table S1 for the numbering of the various experiments and the porphyrins included). The experiments were performed in 384-well plates at 37 °C, with 20 μM peptide concentration. The concentration of porphyrin varied from 0.1 μM to 40 μM depending on the tested porphyrin. All the ThT fluorescence kinetic curves exhibit a typical sigmoidal appearance (Fig. 1 and Fig. S2), characterized by an initial lag phase corresponding to nucleation, a growth phase linked to elongation and secondary nucleation processes, and a final stationary phase. Three key kinetic parameters describing the self-assembly process will be discussed in the following: the difference between the initial and final fluorescence intensities, ΔF; the time at which the fluorescence intensity has increased by $\Delta F/2$, $t_{1/2}$; and the slope at $t_{1/2}$, $k_{t_{1/2}}$. Comparison of the influence of the porphyrins on these kinetic parameters is shown in Fig. 2 (see Fig. S3–S5 for the additional self-assembly experiments). The obtained results highlight the good reproducibility of the trends observed between independent experiments. Besides, TEM and AFM images of the formed assemblies captured at the end of the fluorescence experiments give insights into their morphology and size. They are shown in Fig. 1 and Fig. S6, S7 for the additional self-assembly experiments.

First, the negatively charged porphyrin **H_2-TPPS** was tested at various concentrations (from 2 μM to 40 μM). The self-assembly parameters are virtually identical (Fig. 1A and 2), except for the maximum ThT fluorescence intensity for which a slight decrease is observed. TEM images indicate that the twisted structure built on 3–4 fibrils is conserved even at 10 μM concentration in porphyrin (compare Fig. 1E and Fig. S6B with Fig. 1D and Fig. S6A). Hence, **H_2-TPPS** neither affects the kinetics of Aβ(1–40) self-assembly nor changes the structure of the fibrils, indicating that it does not modify significantly Aβ(1–40) peptide self-assembly in line with reported data on Aβ(1–42).[34]

In contrast to what was observed in the presence of **H_2-TPPS**, significant changes are observed in the Aβ(1–40) self-assembly curves in the presence of cationic porphyrins (Fig. 1B, C and Fig. S2). Their addition leads to a significant acceleration of the Aβ(1–40) self-assembly that depends on the porphyrin nature and concentration as reflected by the corresponding decrease of the $t_{1/2}$ (Fig. 2A and Fig. S4A–S5A). In the case of **H_2-TMPyP**, $t_{1/2}$ decreases with a monotonic concentration dependence with a maximal acceleration effect observed at the highest tested concentration (Fig. 2A and Fig. S4A). In the case of **H_2-MA**, the $t_{1/2}$ decreases until the porphyrin concentration reaches a concentration of 2 μM and again increases at higher concentrations (Fig. 2A and Fig. S5A). The concentration corresponding to the maximal acceleration

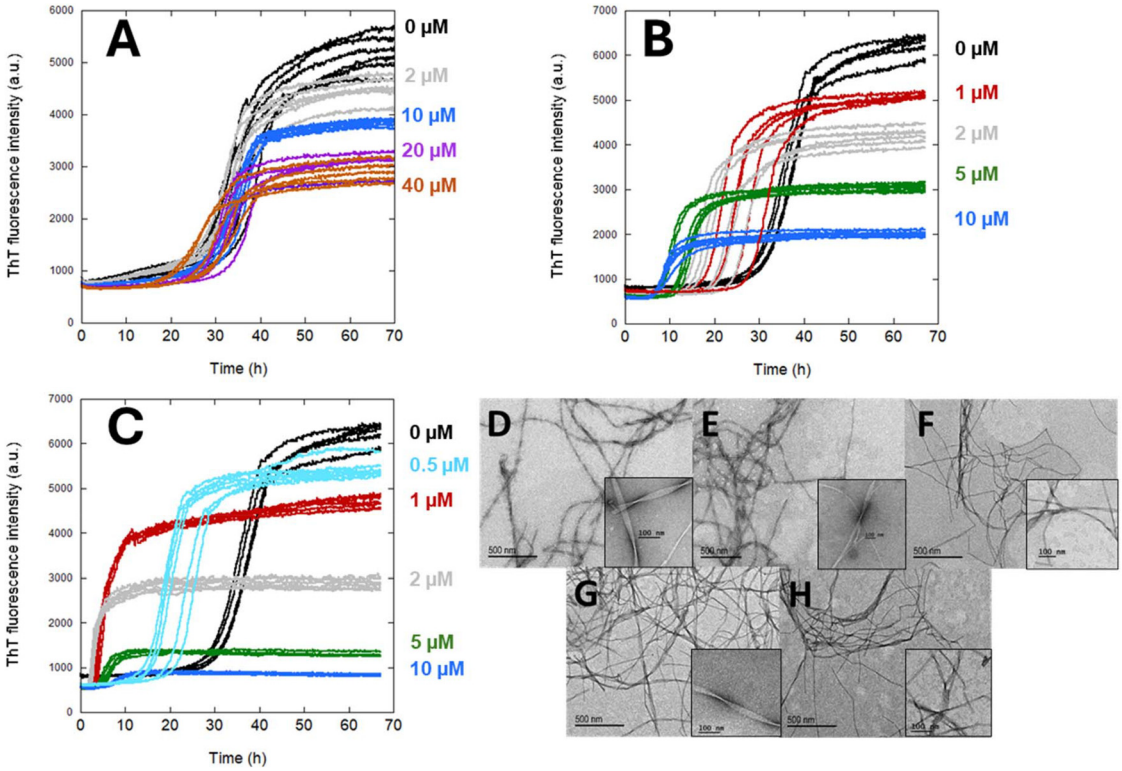

Fig. 1 Self-assembly of the Aβ(1–40) peptide (20 μM) in the presence of various concentrations of porphyrins in 100 mM HEPES buffer, pH 7.4, at 37 °C. ThT fluorescence kinetic curves in the presence of (A) **H_2-TPPS** (from experiment No. 2), (B) **H_2-TMPyP** and (C) **H_2-MA** (from experiment No. 1). Black: Aβ(1–40) peptide; light blue, red, grey, green, dark blue, violet and brown correspond to the presence of 0.5, 1, 2, 5, 10, 20 and 40 μM porphyrin, respectively. Six replicates are shown to illustrate reproducibility. Corresponding TEM images, at two different magnifications, of the fibril morphologies obtained after 3 days: (D) 20 μM Aβ(1–40) and in the presence of (E) 10 μM **H_2-TPPS**, (F) 1 μM **H_2-TMPyP**, (G) 10 μM **H_2-TMPyP**, and (H) 1 μM **H_2-MA**.

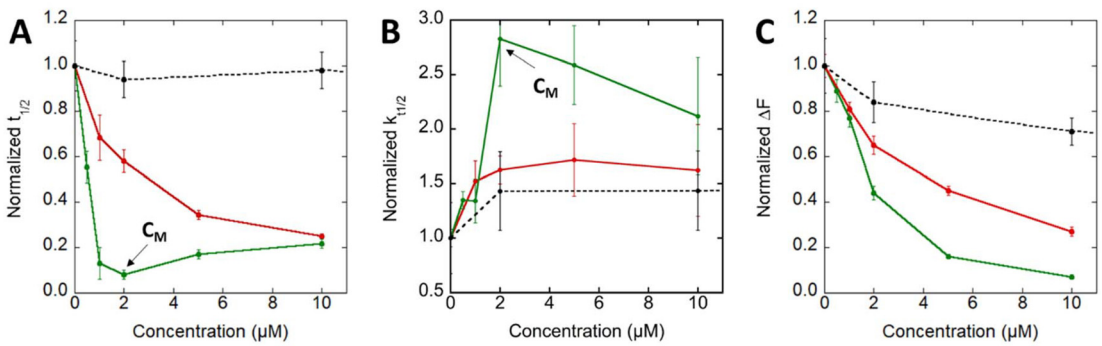

Fig. 2 Kinetic parameters describing the concentration-dependent effects of porphyrins on Aβ(1–40) self-assembly. (A) Normalized $t_{1/2}$; (B) normalized $k_{t_{1/2}}$ and (C) normalized ΔF (normalization is based on the parameters of the peptide alone; see the Experimental section for details). Red: **H_2-TMPyP**, green: **H_2-MA**, and black: **H_2-TPPS**. C_M corresponds to the concentration where the accelerating effect of the porphyrins is maximum. Data are from Fig. 1.

is denoted C_M. The accelerating effects of both porphyrins can be compared at 1 μM. The Aβ(1–40) self-assembly was extremely rapid in the presence of **H_2-MA**, the $t_{1/2}$ being 10 times shorter than that of the control (normalized $t_{1/2}$ = 0.1, Fig. 2A and Fig. S5A), in contrast to **H_2-TMPyP** with a normalized $t_{1/2}$ = 0.7 (Fig. 2A and Fig. S4A). Similar porphyrin-dependent trends are observed for the slope $k_{t_{1/2}}$ of the growth phase. Indeed, **H_2-TMPyP** induced a weak and monotonic increase in $k_{t_{1/2}}$, and **H_2-MA** produced a much steeper increase, maximal at 2 μM, Fig. 2B and Fig. S4–S5B. Monotonic *versus* biphasic variations are thus detected on both the $t_{1/2}$ and $k_{t_{1/2}}$ upon addition of **H_2-TMPyP** and **H_2-MA**, respectively. This indicates that the por-

phyrin's nature and concentration-dependent effects concern not only the nucleation step but also the growth phase of the Aβ(1–40) self-assembly.

Besides, as shown in Fig. 1, 2C and Fig. S4–S5C, a decrease in the maximum fluorescence intensity (F_{max}) with the increase of the porphyrin concentration is observed. It can have several origins: (i) the porphyrins absorb at λ = 440 nm at which ThT is excited. Hence, they can induce a significant inner-filter effect (IFE, which limits the level of absorbed light to excite ThT). The extent of the IFE is dependent on the molar extinction coefficient (ε) of each porphyrin (see Table S2) and on its concentration. The IFE follows the equation $10^{-(abs^* [porph])}$, where abs is a constant value that combines the ε value and the path length. For a given porphyrin, the decrease observed in the ThT fluorescence does not correspond to this law. In addition, the ThT fluorescence decrease does not correspond to the respective ε values of the added porphyrins. More precisely, the effect observed is **H_2-MA** > **H_2-TMPyP** > **H_2-TPPS** although the ε value follows the order **H_2-TMPyP** > **H_2-MA** > **H_2-TPPS**. In addition, the porphyrins undergo a hypochromic effect during interaction with Aβ(1–40) and Aβ(1–40) self-assembly (Fig. 3, *vide infra*) which is stronger for **H_2-MA** *versus* the other two porphyrins. Altogether, this indicates that the IFE is not predominant in the case of **H_2-MA**; (ii) the porphyrins induce the decrease of the number of fibrils formed and/or a change in their morphology, with the formation of Aβ(1–40) fibrils less responsive to ThT; (iii) the porphyrins and ThT compete for the same binding sites within the fibrils. It is likely that the three effects occur. The extent to which they contribute to the observed decrease in ThT fluorescence is extremely difficult to assess quantitatively. Hence, to evaluate the effect of cationic porphyrins on the formation of Aβ(1–40) fibrils, both on the level of fibril formation and/or the morphology, the Aβ(1–40) self-assembly media were collected after four days at 37 °C and were analyzed by microscopic imaging (TEM and AFM). The TEM image of the Aβ(1–40) control shows the classic long twisted assemblies based on 3–4 fibrils of Aβ (Fig. 1D and Fig. S6A).[68] In the presence of 1 μM **H_2-TMPyP** and 10 μM **H_2-TMPyP** (Fig. 1E, F and Fig. S6C, respectively) and 1 μM **H_2-MA** (Fig. 1H and Fig. S6E), thinner assemblies (some of them built on 2 fibrils) are observed with no clear differences between the images. In the medium containing 10 μM **H_2-MA**, no fibrils were found either on the TEM grids (not shown) or on the AFM chips, although they were searched with the greatest care. AFM was also performed at the intermediate concentration of 5 μM to grasp some species with lower molecular weights for **H_2-TMPyP** or **H_2-MA**, and the obtained pictures show the presence of numerous fibrils in the presence of **H_2-TMPyP**, whereas very few fibrils were observed for **H_2-MA** (Fig. S7).

In summary, the cationic porphyrins are able to influence Aβ(1–40) self-assembly by changing its rate and by preventing the formation of fibrils in a concentration-dependent manner. We observe two effects. For **H_2-TMPyP**, a monotonic acceleration of the Aβ(1–40) self-assembly was observed (decrease in $t_{1/2}$, Fig. 2A and Fig. S4A), and the morphology of the fibrils was altered as thinner fibrils were detected by TEM at 1 and 10 μM (Fig. 1F, G and Fig. S6C, D). For **H_2-MA**, the kinetic effect follows a bell-shaped curve (Fig. 2A and Fig. S5A), with maximal acceleration of Aβ(1–40) self-assembly observed at C_M ~ 2 μM. Thinner fibrils were observed by TEM at 1 μM (Fig. 1H and Fig. S6E), and no fibrils were observed at 10 μM.

Interactions of non-metallated porphyrins with monomeric and self-assembled Aβ(1–40)

UV-vis spectroscopy. To probe the interaction between the porphyrins and Aβ, UV-vis absorption spectra of porphyrins were recorded in the absence or presence of monomeric and self-assembled Aβ(1–40) (Fig. 3). The spectra of all the porphyrins remain unchanged in the presence of monomeric Aβ(1–40).

The UV-vis spectra of the anionic porphyrin, **H_2-TPPS**, did not significantly change during the self-assembly of Aβ(1–40) (λ_{max} = 415 nm) (Fig. 3A). In contrast, the spectra recorded at the end of Aβ(1–40) self-assembly in the presence of 2 μM of the other porphyrins show shifted Soret absorbance peak for **H_2-TMPyP**, from 423 to 432 nm ($\Delta\lambda$ = 9 nm) (Fig. 3B) and for **H_2-MA**, from 418 to 424 nm ($\Delta\lambda$ = 6 nm) (Fig. 3C). These bathochromic shifts together with the associated hypochromic effect

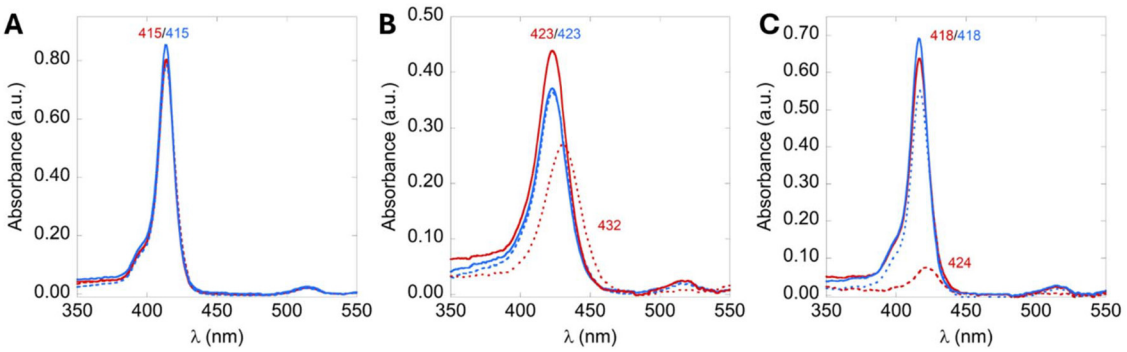

Fig. 3 UV-visible spectra of 2 μM porphyrin with (red) or without Aβ(1–40) (blue), recorded before (solid lines) and at the end of Aβ(1–40) self-assembly (dotted lines). (A) **H_2-TPPS**, (B) **H_2-TMPyP**, and (C) **H_2-MA**. [Aβ(1–40)] = 20 μM, [HEPES] = 100 mM, pH 7.4, T = 37 °C and ℓ = 1 cm.

are typical signatures of the porphyrin macrocycle undergoing π-stacking interactions with its environment.[69,70]

Fluorescence. We then take advantage of the intrinsic fluorescence of non-metallated porphyrins[71–73] to kinetically monitor Aβ(1–40) self-assembly. The changes induced by the peptide self-assembly on the fluorescence were followed at λ_{ex} = 410 nm and λ_{em} = 640 nm (Fig. 4A and Fig. S8, S9). The fluorescence of the porphyrins decreased along a sigmoidal curve reminiscent of that observed for ThT. However, a shorter $t_{1/2}$ is measured, indicating that the events probed precede the formation of the well-organized β-sheet-rich fibrils detected by ThT fluorescence (Fig. 4A and Fig. S8, S9). The difference between the two characteristic times is denoted $\Delta t_{1/2}$ (Fig. 4A). The extent of the decrease in porphyrin fluorescence is about 15% for **H_2-TMPyP** and 65% for **H_2-MA**, while $\Delta t_{1/2}$ is about 0.3 h for **H_2-MA** and null for **H_2-TMPyP** (Fig. 4B and Fig. S8, S9, Table S3) at 5 μM. This may witness the extent of the hydrophobic interactions between the porphyrins and the species formed prior to Aβ(1–40) fibrils (later referred to as nuclei). For **H_2-MA**, but not for **H_2-TMPyP**, which has too weak fluorescence (Fig. S8A), a concentration–dependent study (between 1 and 10 μM) was also performed (Fig. S9 and Table S4). Two trends can be observed: (i) the decrease in porphyrin fluorescence intensity was virtually independent of porphyrin concentration (Table S4) and (ii) $\Delta t_{1/2}$ decreases when the porphyrin concentration increased (Fig. 4B). This indicates that the various equilibria involved in Aβ(1–40) self-assembly are differently altered by porphyrin concentration, with higher concentrations of porphyrin favoring the formation of higher molecular weight species. Overall, the gradual changes in the fluorescence of the porphyrins during fibrillation indicate that they interact with the peptide in a specific environment that does not yet correspond to Aβ(1–40) fibrils. The decrease in porphyrin fluorescence may be related to interactions with Aβ(1–40) intermediate-sized assemblies capable of providing a hydrophobic environment similar to that encountered during intercalation between DNA base pairs.[70]

NMR. The NMR spectra of Aβ(1–40) were recorded in the presence of 0.1 equiv. of **H_2-TPPS**, **H_2-TMPyP** and **H_2-MA** (Fig. 5, see Fig. S10–S13 for other spectral domains and stoichiometries). Attribution of key residues was performed according to the literature.[74–78] In the 7.50–7.70 ppm region, five singlets corresponding to the three Hε protons of His6, His13 and His14 and to two amide NH protons (the first one is from Val40 NH and the second one is not attributed) are detected. The signals between 6.95 and 7.25 ppm are attributed to Phe4, Phe19 and Phe20 residues. Tyr10 aromatic protons appear as two doublets at δ = 6.65 and 6.92 ppm. Finally, three singlets at δ = 6.77, 6.78 and 6.86 ppm corresponding to the three Hδ of His6, His13 and His14 of Aβ(1–40), in addition to two non-attributed amide NH protons, are detected. Upon addition of porphyrins, shifts of all aromatic peaks were observed that are linked to π-stacking interactions between the tetrapyrrolic ring of the porphyrin and the aromatic residues. A stronger shift is detected for **H_2-MA** > **H_2-TMPyP** > **H_2-TPPS**, thus mirroring a stronger interaction between **H_2-MA** and the peptide. Similar trends are observed for Hβ (Fig. S11), the –Me group of Met35 (Fig. S12), and Val12 and Val18 (Fig. S13). This indicates a preferential binding of the porphyrins to the hydrophobic core of the peptide (Scheme 1A). For the three porphyrins, the aromatic His peaks exhibited smaller shifts than the Phe and Tyr ones. This may be related to the partially protonated state of His at pH 7.4 disfavoring the interactions with the cationic porphyrins. NMR confirms the trends previously observed by UV-vis and fluorescence with respect to the strengths of the interactions between the porphyrins and Aβ(1–40).

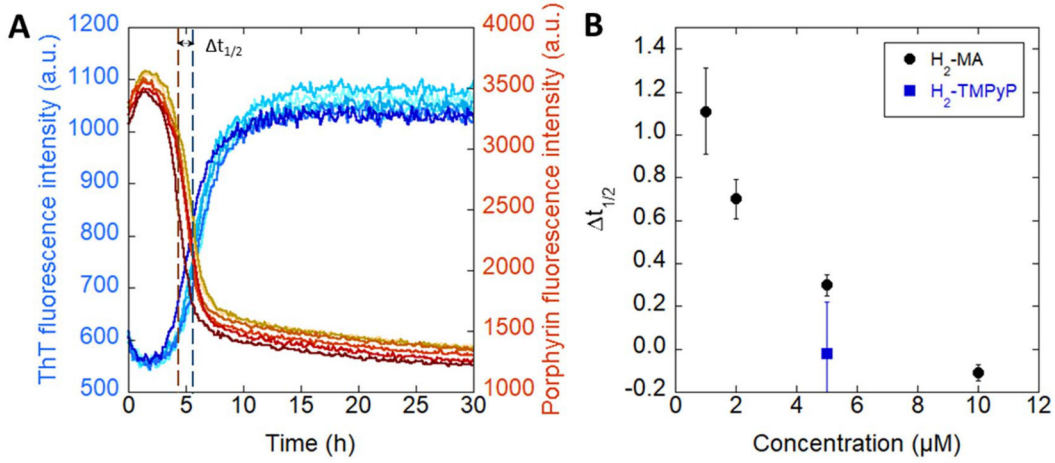

Fig. 4 (A) Kinetic curves of Aβ(1–40) self-assembly (20 μM) in the presence of **H_2-MA** (black circles in panel B) at 5 μM, recorded at λ_{em} = 640 (excitation at λ = 410 nm). Brown traces correspond to the fluorescence of the porphyrin, while blue traces correspond to ThT fluorescence. Lines are replicates from one experiment. (B) Difference between $t_{1/2}$ values detected by the fluorescence of porphyrin (brown dotted line in panel A) and ThT (blue dotted line in panel A) as a function of porphyrin concentration. Black circles: **H_2-MA** at different concentrations; blue square: **H_2-TMPyP** at 5 μM.

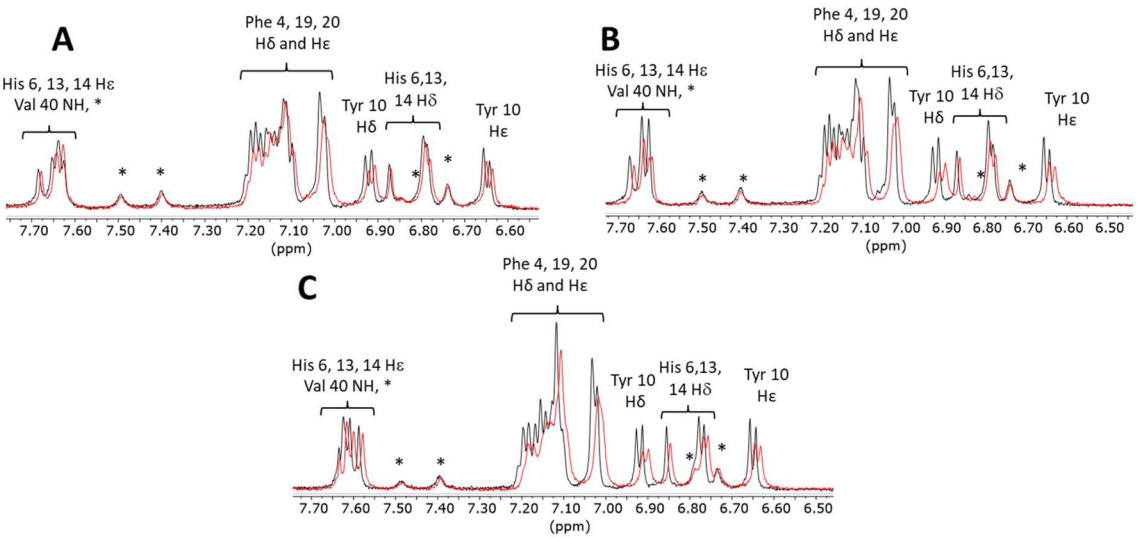

Fig. 5 ^{1}H NMR spectra of the selected aromatic regions of Aβ(1–40) 200 μM, pH 7.4, in 10 mM d^{18}-HEPES buffer (10% D_2O). Control (black trace) and spectra recorded in the presence of 0.1 equiv. (red trace) of added porphyrin: (A) **H_2-TPPS**, (B) **H_2-TMPyP** and (C) **H_2-MA**. Signals marked with * correspond to non-attributed NH amide protons.

Influence of the metallated porphyrins on the fibrillation of Aβ(1–40) peptide

To further investigate and obtain additional data of the interactions with Aβ(1–40), we used Cu(II) and Au(III) derivatives of the cationic porphyrins. Such metalation preserves the flat shape of the porphyrin as no apical ligation occurs,[79,80] but changes the charge (in the case of Au(III)) and lowers the electron density of the aromatic ligand system, thus increasing the π-stacking properties.[81,82]

The effects of pentacationic **Au(III)-MA** and **Au(III)-TMPyP** and tetracationic **Cu(II)-MA** porphyrins (Scheme 2) were tested on the self-assembly of Aβ(1–40) (Fig. S14). In the case of **Au-TMPyP**, the monotonic accelerating effect is stronger than the one detected for **H_2-TMPyP** (Fig. S15A). In the case of **Au-MA**, a concentration dependence similar to that of **H_2-MA** is observed (Fig. 6A, B and Fig. S2C, D) where the threshold value (C_M) is obtained at a lower porphyrin concentration: 1 μM for **Au-MA** *versus* 2 μM for **H_2-MA** (Fig. 7A and Fig. S17A). In the case of **Cu-MA** (Fig. 6C and Fig. S2E), effects similar to those observed for **H_2-MA** are observed. For the three metalated porphyrins, the evolution of the maximal ThT fluorescence values is similar to that of their apo-counterpart (Fig. 7C and Fig. S17, S18C). Among the three possible origins of the observed ThT fluorescence decrease, as described previously, the inner-filter effect may not contribute significantly as the molar extinction coefficient values of the metalated porphyrins are weaker than the free-base porphyrins (Fig. S16 and Table S2).

TEM pictures were captured after the self-assembly of Aβ(1–40) in the presence of 1 μM metallated porphyrin (Fig. 6F, G and Fig. S7F, G). All the porphyrins do induce a change in the morphology of Aβ(1–40) fibrils but to different extents: **Cu-MA** exhibited the same effects as **H_2-MA** exhibited (compare Fig. 6G with Fig. 6E), whereas the fibrils formed in the presence of **Au-MA** were longer and wider and exhibited well-resolved twists and nodes, although they were less numerous (Fig. 6F). At 10 μM metallated porphyrin, no fibrils were detected on the TEM grids. AFM was performed at 5 μM, and spherical and toroidal objects of about 20–40 nm and 30–100 nm were detected for **Cu-MA** and **Au-MA**, respectively (Fig. S19). Hence, the TEM and AFM imaging indicate that the diminution of ThT fluorescence in the case of **Cu-MA** and **Au-MA** is mainly linked to the formation of non-fibrillar species.

In brief, the **Cu(II)-MA** porphyrin has a similar effect on Aβ(1–40) self-assembly to that of **H_2-MA**. This is in line with the two compounds having the same number of charges. In contrast, **Au(III)-MA** increased the capacity of the porphyrin to change the kinetics of Aβ(1–40) self-assembly compared to the non-metallated counterpart. This is due to an extra positive charge and the stronger π-stacking capacity, both properties being anticipated to enhance the interaction with Aβ(1–40).

Interactions of metallated porphyrins with the monomeric and self-assembled Aβ(1–40)

The interactions of the metalated porphyrins were then probed by UV-vis and by ^{1}H NMR (Fig. 8) with the aim of relating them to the impact of the porphyrins on Aβ(1–40) self-assembly. In UV-vis, the trend observed is a bathochromic shift where **Au-MA** > **Cu-MA** ∼ **H_2-MA**, in line with the effects observed on Aβ(1–40) self-assembly. In NMR, the modifications induced in the peptide spectrum depend on the porphyrin under study. In the case of the diamagnetic **Au-MA** (Fig. 8E), shifts of key residues' peaks reminiscent of what was observed previously for **H_2-MA** were detected, although to a greater extent (Fig. 8D). Indeed, 10% of **Au-MA** induces a higher shielding ($\Delta\delta$ ∼ 0.06–0.1 ppm) of the Phe and Tyr aromatic protons and also a stronger broadening, keeping the His

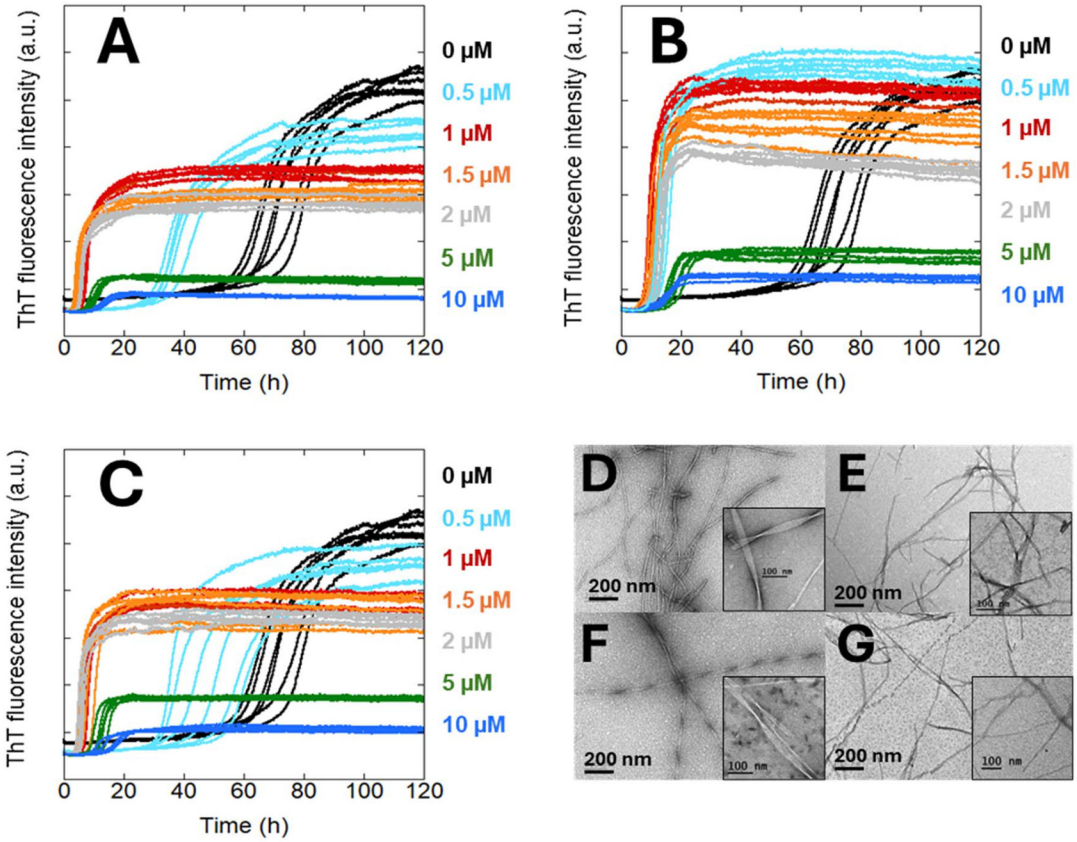

Fig. 6 Self-assembly of the Aβ(1–40) peptide (20 μM) in the presence of various concentrations of porphyrins in 100 mM HEPES buffer, pH 7.4, at 37 °C. ThT fluorescence kinetic curves in the presence of (A) **H_2-MA** (from experiment No. 3), (B) **Au-MA** (from experiment No. 3) and (C) **Cu-MA** (from experiment No. 3). Black: Aβ(1–40) peptide, light blue, red, orange, grey, green and blue correspond to the presence of 0.5, 1, 1.5, 2, 5, and 10 μM porphyrin, respectively. Note that the fluorescence intensity has the same scale for all the graphs. Six replicates are shown to illustrate reproducibility. Corresponding TEM images, at two magnifications, of the fibril morphologies obtained after 3 days: (D) 20 μM Aβ(1–40) and in the presence of (E) 10 μM **H_2-MA**, (F) 1 μM **Au-MA**, and (G) 1 μM **Cu-MA**.

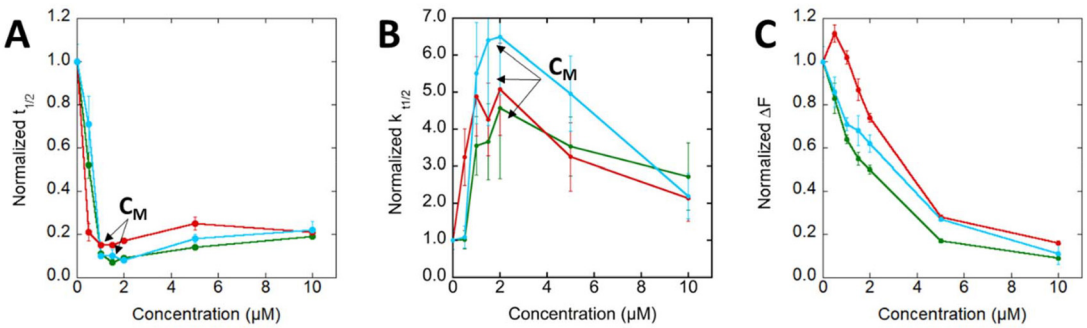

Fig. 7 Kinetic parameters describing the concentration-dependent effects of porphyrins on Aβ(1–40) self-assembly. (A) Normalized $t_{1/2}$; (B) normalized $k_{t_{1/2}}$ and (C) normalized ΔF (normalization is based on the parameters of the peptide alone; see the Experimental section for details). Red: **Au-MA**, green: **H_2-MA**, and blue: **Cu-MA**. C_M corresponds to the concentration where the accelerating effect of the porphyrins is maximum. Data are from Fig. 6.

residues weakly affected (Fig. 8E). In the aliphatic region, the induced shifts of specific peaks (Hβ of Phe20, His6, His13, His14, Tyr10, and Ala (Fig. S21, S22A and B)) and Hγ of Val12 & 18 (Fig. S23A & B) are also stronger for **Au-MA** *versus* **H_2-MA**. The addition of the paramagnetic **Cu-MA** porphyrin leads to broadening effects rather than shifts for the diamagnetic porphyrins previously described.[83] When added at a 2% molar ratio (Fig. 8F), the protons (Hδ and Hε) of the His were not significantly affected, yet the intensity of the Tyr (Hε and Hδ) protons decreased. At 10% **Cu-MA**, the signals of the aromatic

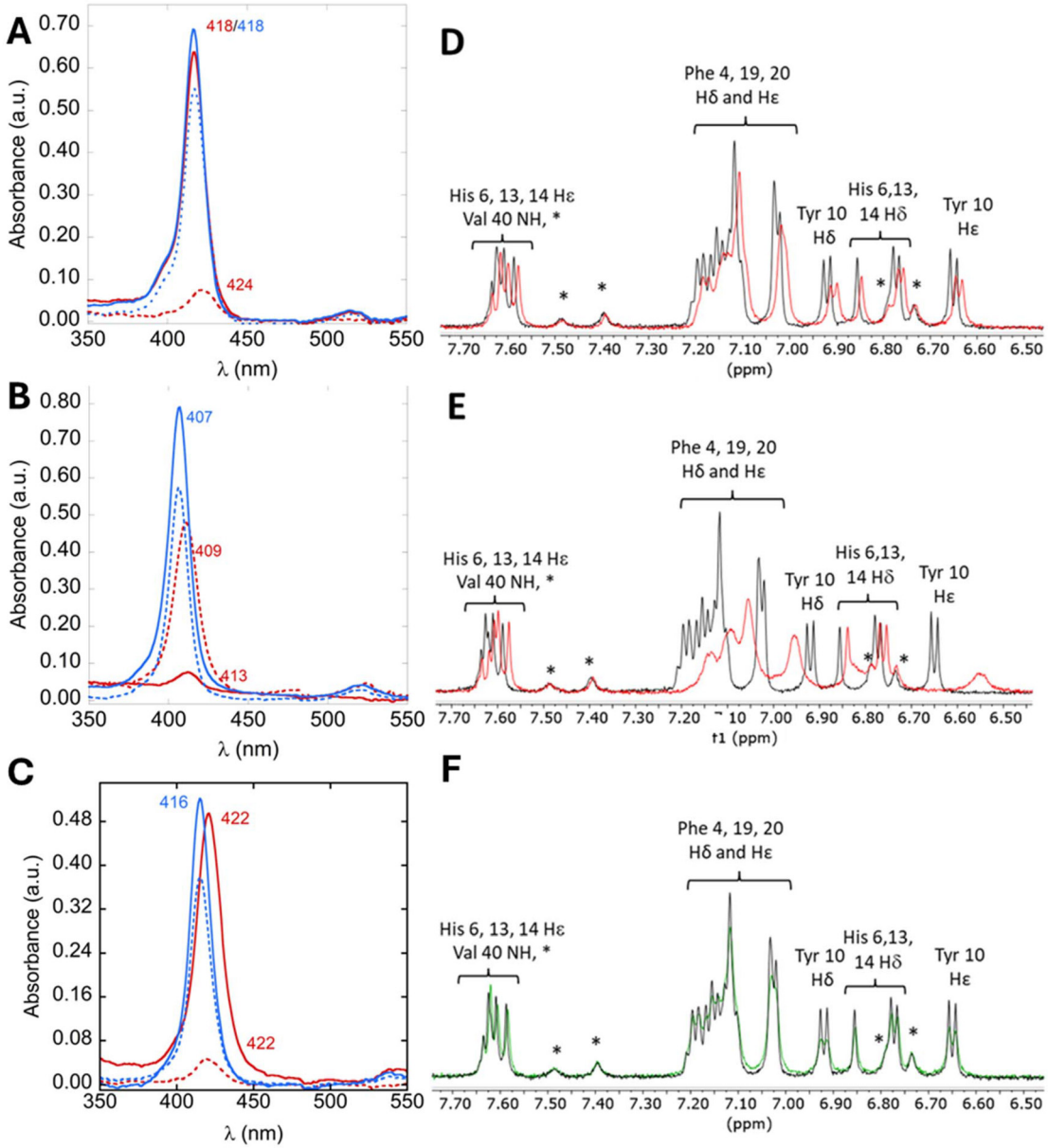

Fig. 8 UV-visible spectra of 2 μM porphyrin with (red) or without Aβ(1–40) (blue), recorded before (solid lines) and at the end of Aβ(1–40) self-assembly (dotted lines). (A) **H_2-MA**, (B) **Au-MA**, and (C) **Cu-MA**. [Aβ(1–40)] = 20 μM, [HEPES] = 100 mM, pH 7.4, T = 37 °C and ℓ = 1 cm. ^{1}H-NMR spectra of selected aromatic regions of Aβ(1–40) 200 μM, pH 7.4, in 10 mM d^{18}-HEPES buffer (10% D_2O). Control (black trace) and spectra recorded in the presence of 0.02 equiv. (green trace) or 0.1 equiv. (red trace) of added porphyrin: (D) **H_2-MA**, (E) **Au-TMPyP** and (F) **Cu-MA**. Signals marked with * correspond to non-attributed NH amide protons.

Phe residues broadened, and the Tyr signals vanished with the His signals remaining less affected (Fig. S20C). Given the fact that Cu(II) does not bind to the Tyr of the Aβ peptide,[84] it is unlikely that Cu(II) inside a porphyrin scaffold does. Hence, the interactions are mainly π-stacking/hydrophobic. For the three Phe residues (Phe4, Phe19, and Phe20), as their signals superimpose, it is difficult to identify whether one or two are more affected than the other(s). In the aliphatic region, strong broadening is also observed for Hβ of His and Tyr (Fig. S21C), for Leu17/34 and Hγ of Val12 and 18, and for the Me group of Met35 (Fig. S22C and S23C). For the three porphyrins, the same residues are affected, mostly lying in the CHC. **Au-MA** had a greater effect than **H_2-MA** in line with stronger interaction by π-stacking and the higher modulation of Aβ(1–40) self-assembly.

Possible mechanisms under study

In the present study that has scrutinized the effects of a family of porphyrins on Aβ(1–40) self-assembly, as well as the interactions between the porphyrins and the peptide, several trends were observed and are summarized and discussed below.

(1) The effect of the porphyrins on Aβ(1–40) self-assembly depends on the chemical nature, which can be gathered into three families. The anionic **H_2-TPPS** porphyrin has virtually no impact on Aβ(1–40) self-assembly. **H_2-TMPyP** and **Au-TMPyP** exert an accelerating effect that monotonically increases with the porphyrin concentration (up to the concentration values studied). Finally, **H_2-MA**, **Cu-MA** and **Au-MA** induce a biphasic trend, for which the accelerating effect reaches a maximum at a given concentration (C_M that generally lies in the 1–2 μM range or, otherwise stated, 0.05–0.1 equiv. per Aβ(1–40) peptide). We propose that the three types of effects observed (no effect, monotonic and biphasic fastening of the assembly) are linked to the strength of the interactions of the porphyrins with the Aβ(1–40) peptide, either in its monomeric form as probed by NMR and UV-Vis (Fig. 3, 5 and 8) or once self-assembled as probed by fluorescence and UV-Vis (Fig. 3, 6 and 8).

(2) The anionic porphyrin weakly interacts with the Aβ(1–40) peptide that is globally negatively charged at neutral pH (overall charge = −2.7) and that possesses a unique cationic residue (Lys16) at the edge of the CHC *versus* two anionic residues in the middle of the CHC (Scheme 1B). The cationic porphyrins have effects that depend on the length of the cationic arms, with **H_2-MA** exhibiting stronger effects than **H_2-TMPyP** on Aβ(1–40) self-assembly (Fig. 1 and 2).

(3) **Cu-MA** porphyrin shows a similar accelerating effect on Aβ(1–40) self-assembly as the parent **H_2-MA**; a stronger effect is observed for **Au-MA** in line with the higher hydrophobicity of the aromatic ring and a higher number of positive charges.

We propose that the cationic porphyrins interact in the CHC of the Aβ(1–40) peptide and that two main forces are important:

(i) The hydrophobicity (**H_2-TMPyP** < **H_2-MA** ∼ **Cu-MA** < **Au-MA**) and the resulting stacking interactions with the aromatic residues (Phe 19 & 20) and hydrophobic interactions with Val12 and Val18 and Leu17 as probed by NMR (Fig. 5, 8 and Fig. S10–S13, S20–S23).

(ii) The electrostatic interactions with anionic residues (mainly Glu22 and Asp23) are expected to increase with the accessibility of the porphyrin cationic arms (**H_2-TMPyP** < **H_2-MA**). The stronger these interactions are, the stronger the effects on the kinetics of Aβ(1–40) self-assembly and on the prevention of fibril formation (Fig. 1, 6 and Fig. S6, S7, S19).

Scheme 3 represents the proposed main site of interactions of each porphyrin with the Aβ(1–40) peptide; a possible secondary site of interactions is shown in Scheme S1. We used the rough diameter of porphyrins to estimate the porphyrin/peptide ratio.[33] According to a very simplified estimation, about 4 and 5 peptides should be required to host **H_2-TMPyP** and **H_2-MA**, respectively.

Furthermore, to explain the changes induced by the porphyrins on the Aβ(1–40) self-assembly, we propose a simplified mechanism, shown in Scheme 4 for the **MA** family, where 6 equilibria are involved. The interactions of the Aβ(1–40) peptide and the porphyrins lead to the formation of nuclei, which is faster and/or more favored than in the absence of porphyrin (Scheme 1B *versus* Scheme 4, eq. 1)). This may be due to the fact that porphyrins help several peptides to be gathered and/or to be oriented in a way more favorable for self-assembly. As a reminder, several peptides are required to host one porphyrin, with the ratio values that depend on the size of the porphyrin (Scheme 3). Then, two elongation paths may coexist: (i) in the first one, Aβ(1–40) is added at the extremities of the nuclei. Because the nuclei are different from those obtained in the absence of porphyrins, they may be more prone to elongate (eq. 2); (ii) the second one (eq. 3), the addition of Aβ(1–40) at the extremities is promoted by the presence of the porphyrins. Eq. 2 and 3 contribute to the faster elongation rates observed in the presence of cationic porphyrins (Fig. 6 and Fig. S2) up to about the C_M concentration. Note that the interaction of the cationic porphyrins with assemblies of 4 to 5 peptides, as probed by the decrease in their intrinsic fluorescence and preceding the formation of ThT-responsive fibrils, may correspond to the formation of nuclei (eq. 1). In addition, the higher the porphyrin concentration is, the shorter the time difference between the formation of nuclei and that of ThT-responsive fibrils is (Fig. 4). Considering that porphyrin fluorescence reflects the formation of nuclei, such a concentration-dependent trend may indicate that eq. 3 (dependent on porphyrin concentration) contributes more to the whole assembly process than eq. 2 (independent of porphyrin concentration). Porphyrin interactions with formed fibrils can

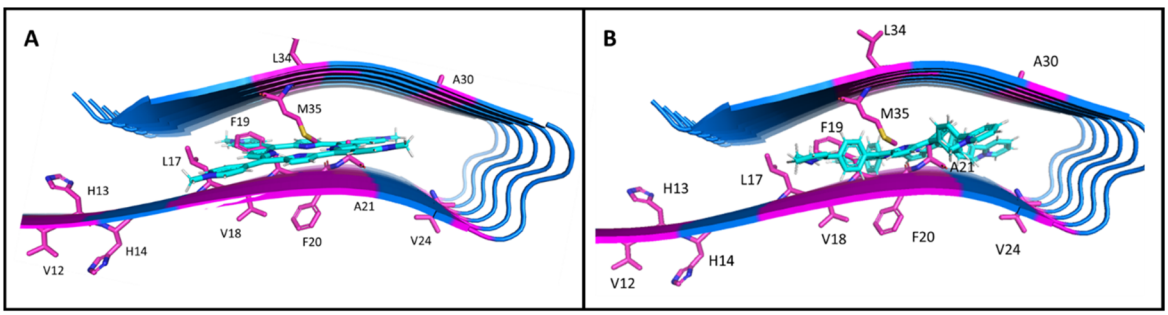

Scheme 3 Representation of the interactions of the porphyrins with the Aβ(1–40) peptide. (A) **H_2-TMPyP** and (B) the **MA** family. Drawings were generated based on 5 Aβ(1–40) using AlphaFold 3.[85] Interacting amino acids are shown in pink.

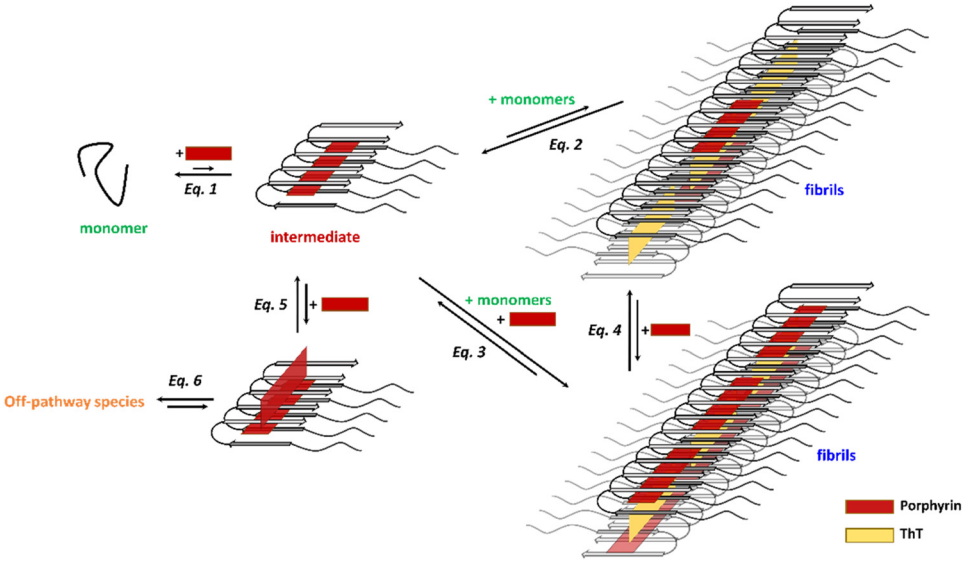

Scheme 4 Simplified mechanism to explain the effects of **MA**-family porphyrins on Aβ(1–40) self-assembly. Red rectangles = porphyrins and yellow rectangles = ThT.

also occur (eq. 4). Note that, in this case, we cannot rule out that they substitute ThT from its binding site (as will be described later for **H_2-TMPyP**). Eq. 1–4 are responsible for the shorter $t_{1/2}$ observed in the presence of porphyrins compared to the apo Aβ(1–40) although modifications in secondary nucleation processes may also participate.[17–23] Finally, eq. 5 and 6 correspond to the filling of a second lower-affinity site in the nuclei that may correspond to the ThT binding site[86,87] (eq. 5) and to the further formation of off-pathway aggregates that are not detected by TEM and are responsible for the ThT fluorescence loss (eq. 6). The bulkiness of the **MA** family porphyrins prevents the formation of the cross-β-sheet structure of the fibrils.[88,89] Indeed, they are expected to insert into the groove made by hydrophobic residues involved in the inter-strand formation perpendicular to the axis of fibrils.[90] As the distance between two strands is 11 Å, this does not leave enough space for **MA** insertion without disrupting the inter-strand peptide interactions (Scheme S2). The threshold value for which the concentration of porphyrin leads to the maximal fastening effects mainly corresponds to the balance between two factors: (i) the fastening effects previously described (eqn (1)–(4)), which are higher for **Au-MA** *versus* **H_2-MA** and **Cu-MA** and (ii) the formation of off-pathway aggregates (eqn (5) and (6)).

For **H_2-TMPyP** and **Au-TMPyP** (Scheme S3), the preference for binding to site 1 (eqn (1), and thus eqn (2)–(4)) *versus* site 2 (eqn (5)) is weaker than for the **MA** porphyrins, in line with a weaker fastening of Aβ(1–40) self-assembly. In addition, eqn (5) can exist without leading to off-pathway aggregates because **H_2-TMPyP** is smaller and can insert between the strands, leading to 2 **H_2-TMPyP** per 4 peptides into the fibrils (Scheme S2) as shown by the detection in TEM and AFM of fibrils even at 10 μM **H_2-TMPyP** (Fig. 1–6 and Fig. S6, S7, S19). In this case, the decrease observed in the maximal ThT intensity can be explained by the removal of the ThT from its interaction site that corresponds to the second interaction site of the porphyrin (Scheme S2).[91]

Concluding remarks

In the present article, we report the concentration-dependent effects of a broad series of porphyrins on Aβ(1–40) self-assembly. We propose a structure–activity relationship (SAR), in which the nature of the porphyrin (charge, size and metal ions inserted) is key for the modulation of Aβ(1–40) self-assembly. Various interactions occur to different extents, with electrostatic forces being more important than hydrophobic and/or π-stacking ones (no effect of the anionic porphyrins in contrast to the cationic porphyrins). The size of the porphyrin is also crucial. In the case of **H_2-TMPyP**, the fibrils can host two porphyrins per four peptides into two different binding sites. In the case of bulkier **MA** porphyrins, only the first site is filled with a porphyrin : peptide ratio that cannot exceed 1 : 5 based on geometrical constraints, while the filling of the second site leads to the formation of off-pathway aggregates. Fastening of the self-assembly is due to the preferential binding of the porphyrins into the first site where they gather and/or structure several peptides, which is more favorable to **MA** compared to **H_2-TMPyP**. No coordination interactions were observed for the chosen metalated porphyrins, in line with the absence of apical binding sites. Metalation of the porphyrins with Au(III), in contrast to Cu(II), induces a stronger accelerating effect of Aβ(1–40) self-assembly due to the higher charge and hydrophobicity.

Most studies related to the modulation of amyloid-forming assemblies have focused on porphyrins at a single molar equivalent, thus overlooking concentration-dependent behaviours.[35,37,38,41,43–46,53,64,65,92,93] When concentration-dependent studies were conducted, a slowdown in kinetics

accompanied by inhibition of the self-assembly was reported.[39,42,47] In contrast, we have evidenced here that the ratio between the porphyrin and the peptides is a crucial parameter to guide the modulatory effect on the Aβ(1–40) self-assembly. At low ratios (<0.1 equiv. of porphyrin *versus* peptide), a fastening effect is observed, and at higher ratios, the inhibition of fibril formation is detected for the **MA** series. We thus pointed out that beyond the nature of the modulator, the ratio with respect to the targeted peptide also has to be tightly controlled. Beyond porphyrins, only a few studies report the dependence of Aβ(1–40)/Aβ(1–42) self-assembly as a function of a large range of modulator concentrations,[94–96] and a unique other case of a biphasic trend was described.[94]

In light of the results found in the present article, the interaction of heme with Aβ, which has attracted much attention, might be revisited. Heme has been found to co-localize with Aβ plaques in the cerebral cortex of post-mortem AD brains and was earlier shown to inhibit Aβ aggregation.[35,37,38] The best-characterized interaction of heme with Aβ peptides so far is its coordination with the His residues,[49,50] which was not detected here because the Cu(II)- and Au(III)-substituted porphyrins have no apical ligation site. From studies with mutated Aβ(1–40), residues Phe19 and Phe20 were both shown to be involved in the interaction of heme with Aβ(1–40),[36] which is also detected here. However, rather than the 1 : 1 (heme : Aβ(1–40)) species as currently described,[36,50,97–100] one may consider different interaction ratios in line with our concentration-dependent study.

Last but not least, the quest for Aβ assembly modulators, beyond the insights they can provide into the Aβ assembly itself, remains justified by the continuing need for therapeutic options capable of controlling the deleterious assembly process. Here, we have identified important molecular features and provided a coherent mechanism of action, evidencing that not only the chemical nature of the modulator but also its ratio *versus* peptide matters. Among the key factors involved, the importance of the overall charge of the peptide *versus* the porphyrin is currently being confirmed by the study on positively charged peptides. It would also be of great interest to decipher the role of apical ligation as anticipated based on the interaction of heme with Aβ.

Conflicts of interest

There are no conflicts of interest to declare.

Abbreviations

AD	Alzheimer's disease
Aβ	Amyloid β peptide
CHC	Central hydrophobic core
SAR	Structure–activity relationship
ThT	Thioflavin T
Tyr	Tyrosine
EDTA	Ethylenediaminetetraacetic acid
a.u	Arbitrary units
TEM	Transmission electron microscopy
AFM	Atomic force microscopy
NMR	Nuclear magnetic resonance
C_M	Concentration threshold
ε	Molar extinction coefficient
DNA	Deoxyribonucleic acid
Val	Valine
Phe	Phenylalanine
His	Histidine
Me	Methyl
Met	Methionine
Au	Gold
Cu	Copper
Ala	Alanine
Leu	Leucine
Eq.	Equilibrium

Data availability

The authors state that the data are available in the supplementary information (SI) and upon request from the corresponding author.

Supplementary information is available. See DOI: **https://doi.org/10.1039/d6qi00446f**.

Acknowledgements

The authors acknowledge Lucie de Cremoux for recording the TEM images, David Schmitt for his help in the kinetic data automated mathematical treatment and all the members of the research team for fruitful discussions. The authors would like to acknowledge the METi imaging facility, a member of the national infrastructure France-BioImaging, supported by the French National Research Agency (ANR-10-INBS-04). Financial support from ANR-16-CE18-0022 (project DIVA), ANR-22-CE44-0002-02 (project MASAI), and ANR-21-CE06-0030-01 (project SUPRAMY) is acknowledged.

References

1 C. Wells, S. Brennan, M. Keon and L. Ooi, The role of amyloid oligomers in neurodegenerative pathologies, *Int. J. Biol. Macromol.*, 2021, **181**, 582–604.
2 M. G. Iadanza, M. P. Jackson, E. W. Hewitt, N. A. Ranson and S. E. Radford, A new era for understanding amyloid structures and disease, *Nat. Rev. Mol. Cell Biol.*, 2018, **19**(12), 755–773.
3 Z. L. Almeida and R. M. M. Brito, Structure and Aggregation Mechanisms in Amyloids, *Molecules*, 2020, **25**(5), 1195.

4 P. C. Ke, M.-A. Sani, F. Ding, A. Kakinen, I. Javed, F. Separovic, T. P. Davis and R. Mezzenga, Implications of peptide assemblies in amyloid diseases, *Chem. Soc. Rev.*, 2017, **46**(21), 6492–6531.
5 P. C. Ke, R. Zhou, L. C. Serpell, R. Riek, T. P. J. Knowles, H. A. Lashuel, E. Gazit, I. W. Hamley, T. P. Davis, M. Fändrich, D. E. Otzen, M. R. Chapman, C. M. Dobson, D. S. Eisenberg and R. Mezzenga, Half a century of amyloids: past, present and future, *Chem. Soc. Rev.*, 2020, **49**(15), 5473–5509.
6 D. J. Selkoe and J. Hardy, The amyloid hypothesis of Alzheimer's disease at 25 years, *EMBO Mol. Med.*, 2016, **8**(6), 595–608.
7 Y. Zhang, H. Chen, R. Li, K. Sterling and W. Song, Amyloid β-based therapy for Alzheimer's disease: challenges, successes and future, *Signal Transduction Targeted Ther.*, 2023, **8**(1), 248.
8 A. R. Monteiro, D. J. Barbosa, F. Remião and R. Silva, Alzheimer's disease: Insights and new prospects in disease pathophysiology, biomarkers and disease-modifying drugs, *Biochem. Pharmacol.*, 2023, **211**, 115522.
9 B.-H. Kim, S. Kim, Y. Nam, Y. H. Park, S. M. Shin and M. Moon, Second-generation anti-amyloid monoclonal antibodies for Alzheimer's disease: current landscape and future perspectives, *Transl. Neurodegener.*, 2025, **14**(1), 6.
10 M. Jucker and L. C. Walker, Alzheimer's disease: From immunotherapy to immunoprevention, *Cell*, 2023, **186**(20), 4260–4270.
11 E. Atrián-Blasco, P. Gonzalez, A. Santoro, B. Alies, P. Faller and C. Hureau, Cu and Zn coordination to amyloid peptides: From fascinating chemistry to debated pathological relevance, *Coord. Chem. Rev.*, 2018, **375**, 38–55.
12 C. Hureau, Role of Metal Ions in Alzheimer's Disease: Mechanistic Aspects Contributing to Neurotoxicity, in *Alzheimer's Disease: Recent Findings in Pathophysiology, Diagnostic and Therapeutic Modalities*, ed. T. Govindaraju, The Royal Society of Chemistry, 2022, ch. 7, pp. 170–192.
13 K. E. Marshall, K. L. Morris, D. Charlton, N. O'Reilly, L. Lewis, H. Walden and L. C. Serpell, Hydrophobic, Aromatic, and Electrostatic Interactions Play a Central Role in Amyloid Fibril Formation and Stability, *Biochemistry*, 2011, **50**(12), 2061–2071.
14 T. A. Enache, A.-M. Chiorcea-Paquim and A. M. Oliveira-Brett, Amyloid Beta Peptide VHHQ, KLVFF, and IIGLMVGGVV Domains Involved in Fibrilization: AFM and Electrochemical Characterization, *Anal. Chem.*, 2018, **90**(3), 2285–2292.
15 A. B. Reiss, H. A. Arain, M. M. Stecker, N. M. Siegart and L. J. Kasselman, Amyloid toxicity in Alzheimer's disease, *Rev. Neurosci.*, 2018, **29**(6), 613–627.
16 M. Rana and A. K. Sharma, Cu and Zn interactions with Aβ peptides: consequence of coordination on aggregation and formation of neurotoxic soluble Aβ oligomers, *Metallomics*, 2018, **11**(1), 64–84.
17 M. Törnquist, T. C. T. Michaels, K. Sanagavarapu, X. Yang, G. Meisl, S. I. A. Cohen, T. P. J. Knowles and S. Linse, Secondary nucleation in amyloid formation, *Chem. Commun.*, 2018, **54**(63), 8667–8684.
18 S. Linse, Toward the equilibrium and kinetics of amyloid peptide self-assembly, *Curr. Opin. Struct. Biol.*, 2021, **70**, 87–98.
19 G. Meisl, T. P. J. Knowles and D. Klenerman, Mechanistic Models of Protein Aggregation Across Length-Scales and Time-Scales: From the Test Tube to Neurodegenerative Disease, *Front. Neurosci.*, 2022, **16**, 909861.
20 P. Faller and C. Hureau, Reproducibility Problems of Amyloid-β Self-Assembly and How to Deal With Them, *Front. Chem.*, 2021, **8**, 611227.
21 S. J. C. Lee, E. Nam, H. J. Lee, M. G. Savelieff and M. H. Lim, Towards an understanding of amyloid-β oligomers: characterization, toxicity mechanisms, and inhibitors, *Chem. Soc. Rev.*, 2017, **46**(2), 310–323.
22 S. Linse, Monomer-dependent secondary nucleation in amyloid formation, *Biophys. Rev.*, 2017, **9**(4), 329–338.
23 A. K. Srivastava, J. M. Pittman, J. Zerweck, B. S. Venkata, P. C. Moore, J. R. Sachleben and S. C. Meredith, β-Amyloid aggregation and heterogeneous nucleation, *Protein Sci.*, 2019, **28**(9), 1567–1581.
24 J. Bieschke, M. Herbst, T. Wiglenda, R. P. Friedrich, A. Boeddrich, F. Schiele, D. Kleckers, J. M. Lopez del Amo, B. A. Grüning, Q. Wang, M. R. Schmidt, R. Lurz, R. Anwyl, S. Schnoegl, M. Fändrich, R. F. Frank, B. Reif, S. Günther, D. M. Walsh and E. E. Wanker, Small-molecule conversion of toxic oligomers to nontoxic β-sheet–rich amyloid fibrils, *Nat. Chem. Biol.*, 2012, **8**(1), 93–101.
25 J. Habchi, S. Chia, R. Limbocker, B. Mannini, M. Ahn, M. Perni, O. Hansson, P. Arosio, J. R. Kumita, P. K. Challa, S. I. A. Cohen, S. Linse, C. M. Dobson, T. P. J. Knowles and M. Vendruscolo, Systematic development of small molecules to inhibit specific microscopic steps of Aβ42 aggregation in Alzheimer's disease, *Proc. Natl. Acad. Sci. U. S. A.*, 2017, **114**(2), E200–E208.
26 D. Maity, Inhibition of Amyloid Protein Aggregation Using Selected Peptidomimetics, *ChemMedChem*, 2023, **18**(2), e202200499.
27 D. Maity, Recent advances in the modulation of amyloid protein aggregation using the supramolecular host-guest approaches, *Biophys. Chem.*, 2023, **297**, 107022.
28 R. Roy and S. Paul, Illustrating the Effect of Small Molecules Derived from Natural Resources on Amyloid Peptides, *J. Phys. Chem. B*, 2023, **127**(3), 600–615.
29 R. Perneczky, F. Jessen, T. Grimmer, J. Levin, A. Flöel, O. Peters and L. Froelich, Anti-amyloid antibody therapies in Alzheimer's disease, *Brain*, 2023, **146**(3), 842–849.
30 X. Shao, C. Yan, C. Wang, C. Wang, Y. Cao, Y. Zhou, P. Guan, X. Hu, W. Zhu and S. Ding, Advanced nanomaterials for modulating Alzheimer's related amyloid aggregation, *Nanoscale Adv.*, 2023, **5**(1), 46–80.
31 L. M. F. Gomes, J. C. Bataglioli and T. Storr, Metal complexes that bind to the amyloid-β peptide of relevance to Alzheimer's disease, *Coord. Chem. Rev.*, 2020, **412**, 213255.

32 J. Yoo, J. Lee, B. Ahn, J. Han and M. H. Lim, Multi-target-directed therapeutic strategies for Alzheimer's disease: controlling amyloid-β aggregation, metal ion homeostasis, and enzyme inhibition, *Chem. Sci.*, 2025, **16**(5), 2105–2135.

33 Y. Fan, D. Wu, X. Yi, H. Tang, L. Wu, Y. Xia, Z. Wang, Q. Liu, Z. Zhou and J. Wang, TMPyP Inhibits Amyloid-beta Aggregation and Alleviates Amyloid-Induced Cytotoxicity, *ACS Omega*, 2017, **2**(8), 4188–4195.

34 B. I. Lee, S. Lee, Y. S. Suh, J. S. Lee, A. K. Kim, O. Y. Kwon, K. Yu and C. B. Park, Photoexcited Porphyrins as a Strong Suppressor of beta-Amyloid Aggregation and Synaptic Toxicity, *Angew. Chem., Int. Ed.*, 2015, **54**(39), 11472–11476.

35 D. Howlett, P. Cutler, S. Heales and P. Camilleri, Hemin and related porphyrins inhibit beta-amyloid aggregation, *FEBS Lett.*, 1997, **417**(2), 249–251.

36 C. Yuan and Z. Gao, Abeta interacts with both the iron center and the porphyrin ring of heme: mechanism of heme's action on Abeta aggregation and disaggregation, *Chem. Res. Toxicol.*, 2013, **26**(2), 262–269.

37 S. Taniguchi, N. Suzuki, M. Masuda, S. Hisanaga, T. Iwatsubo, M. Goedert and M. Hasegawa, Inhibition of heparin-induced tau filament formation by phenothiazines, polyphenols, and porphyrins, *J. Biol. Chem.*, 2005, **280**(9), 7614–7623.

38 M. Masuda, N. Suzuki, S. Taniguchi, T. Oikawa, T. Nonaka, T. Iwatsubo, S. Hisanaga, M. Goedert and M. Hasegawa, Small molecule inhibitors of alpha-synuclein filament assembly, *Biochemistry*, 2006, **45**(19), 6085–6094.

39 C. Dong, C. R. Garen, P. Mercier, N. O. Petersen and M. T. Woodside, Characterizing the inhibition of α-synuclein oligomerization by a pharmacological chaperone that prevents prion formation by the protein PrP, *Protein Sci.*, 2019, **28**(9), 1690–1702.

40 N. González, I. Gentile, H. A. Garro, S. Delgado-Ocaña, C. F. Ramunno, F. A. Buratti, C. Griesinger and C. O. Fernández, Metal coordination and peripheral substitution modulate the activity of cyclic tetrapyrroles on αS aggregation: a structural and cell-based study, *J. Biol. Inorg. Chem.*, 2019, **24**(8), 1269–1278.

41 L. Fonseca-Ornelas, S. E. Eisbach, M. Paulat, K. Giller, C. O. Fernández, T. F. Outeiro, S. Becker and M. Zweckstetter, Small molecule-mediated stabilization of vesicle-associated helical α-synuclein inhibits pathogenic misfolding and aggregation, *Nat. Commun.*, 2014, **5**(1), 5857.

42 S. Nath, P. Roy, R. Mandal, R. Roy, A. K. Buell, N. Sengupta and P. K. Tarafdar, Hydroxy-Porphyrin as an Effective, Endogenous Molecular Clamp during Early Stages of Amyloid Fibrillization, *Chem. – Asian J.*, 2021, **16**(23), 3931–3936.

43 S. Chernii, M. Losytskyy, A. Kelm, A. Gorski, I. Tretyakova, S. Yarmoluk, V. Chernii and V. Kovalska, Study of tetraphenylporphyrins as modifiers of insulin amyloid aggregation, *J. Mol. Recognit.*, 2020, **33**(1), e2811.

44 J. Wu, J. Zhao, Z. Yang, H. Li and Z. Gao, Strong Inhibitory Effect of Heme on hIAPP Fibrillation, *Chem. Res. Toxicol.*, 2017, **30**(9), 1711–1719.

45 P. Zhang, L. Zeng, W. Gao, H. Li and Z. Gao, Peroxynitrite scavenger FeTPPS effectively inhibits hIAPP aggregation and protects against amyloid induced cytotoxicity, *Int. J. Biol. Macromol.*, 2020, **161**, 336–344.

46 J. Wu, X. Yin, H. Ye, Z. Gao and H. Li, Structure relationship of metalloporphyrins in inhibiting the aggregation of hIAPP, *Int. J. Biol. Macromol.*, 2021, **167**, 141–150.

47 X. Zhou, L. Zhang, J. Zhi, L. Zhao, R. Shen, A. Yang and X. Kou, Zinc-porphyrin complex as multifunctional anti-AD agent: Synthesis, X-ray single crystal analysis and activity study, *J. Inorg. Biochem.*, 2026, 113245.

48 C. Dey, M. Roy, P. Pal, R. Ghosh and S. G. Dey, Mechanism of oxidative stress and neurotoxicity associated with heme and copper–Aβ relevant to Alzheimer's disease, *Chem. Soc. Rev.*, 2025, **54**(20), 9457–9499.

49 T. L. Poulos, Heme Enzyme Structure and Function, *Chem. Rev.*, 2014, **114**(7), 3919–3962.

50 M. Roy, A. K. Nath, I. Pal and S. G. Dey, Second Sphere Interactions in Amyloidogenic Diseases, *Chem. Rev.*, 2022, **122**(14), 12132–12206.

51 I. Pal and S. G. Dey, The Role of Heme and Copper in Alzheimer's Disease and Type 2 Diabetes Mellitus, *JACS Au*, 2023, **3**(3), 657–681.

52 V. Villari, R. Tosto, G. Di Natale, A. Sinopoli, M. F. Tomasello, S. Lazzaro, N. Micali and G. Pappalardo, A Metalloporphyrin-Peptide Conjugate as an Effective Inhibitor of Amyloid-β Peptide Fibrillation and Cytotoxicity, *ChemistrySelect*, 2017, **2**(28), 9122–9129.

53 W. Xu, C. Gao, X. Sun, W. C.-S. Tai, H. L. Lung and G.-L. Law, Design, synthesis and comparison of water-soluble phthalocyanine/porphyrin analogues and their inhibition effects on Aβ42 fibrillization, *Inorg. Chem. Front.*, 2021, **8**(14), 3501–3513.

54 L. Wang, K. Eom and T. Kwon, Different Aggregation Pathways and Structures for Aβ40 and Aβ42 Peptides, *Biomolecules*, 2021, **11**(2), 198.

55 G. Meisl, X. Yang, E. Hellstrand, B. Frohm, J. B. Kirkegaard, S. I. A. Cohen, C. M. Dobson, S. Linse and T. P. J. Knowles, Differences in nucleation behavior underlie the contrasting aggregation kinetics of the Aβ40 and Aβ42 peptides, *Proc. Natl. Acad. Sci. U. S. A.*, 2014, **111**(26), 9384–9389.

56 C. Romera, L. Sabater, A. Garofalo, I. M. Dixon and G. Pratviel, Interaction of cationic nickel and manganese porphyrins with the minor groove of DNA, *Inorg. Chem.*, 2010, **49**(18), 8558–8567.

57 A. Pipier, A. De Rache, C. Modeste, S. Amrane, E. Mothes-Martin, J.-L. Stigliani, P. Calsou, J.-L. Mergny, G. Pratviel and D. Gomez, G-Quadruplex binding optimization by gold(III) insertion into the center of a porphyrin, *Dalton Trans.*, 2019, **48**(18), 6091–6099.

58 D. Dobrovodsky, A. Danhel, E. Mothes-Martin, G. Pratviel, J.-L. Mergny and M. Fojta, Voltammetric studies of

selected porphyrin G-quadruplex ligands and their interaction with DNA in solution and at the mercury electrode surface, *Electrochim. Acta*, 2021, **394**, 139151.

59 A. Conte-Daban, V. Ambike, R. Guillot, N. Delsuc, C. Policar and C. Hureau, A Metallo Pro-Drug to Target Cu (II) in the Context of Alzheimer's Disease, *Chem. – Eur. J.*, 2018, **24**(20), 5095–5099.

60 L. de Cremoux, E. Falcone, D. Schmitt, E. Stefaniak, M. D. Wiśniewska, N. Vitale, W. Bal and C. Hureau, Modulation of Aβ1–40 and Aβ4–40 co-assembly by zinc: getting closer to the biological reality, *Inorg. Chem. Front.*, 2025, **12**(23), 7827–7844.

61 P. Faller, C. Hureau, P. Dorlet, P. Hellwig, Y. Coppel, F. Collin and B. Alies, Methods and techniques to study the bioinorganic chemistry of metal–peptide complexes linked to neurodegenerative diseases, *Coord. Chem. Rev.*, 2012, **256**(19), 2381–2396.

62 A. Conte-Daban, A. Day, P. Faller and C. Hureau, How Zn can impede Cu detoxification by chelating agents in Alzheimer's disease: a proof-of-concept study, *Dalton Trans.*, 2016, **45**(39), 15671–15678.

63 I. M. Dixon, F. Lopez, A. M. Tejera, J. P. Esteve, M. A. Blasco, G. Pratviel and B. Meunier, A G-quadruplex ligand with 10000-fold selectivity over duplex DNA, *J. Am. Chem. Soc.*, 2007, **129**(6), 1502–1503.

64 Q. Zhang, Y. Liu, J. Wu, L. Zeng, J. Wei, S. Fu, H. Ye, H. Li and Z. Gao, Structure and mechanism behind the inhibitory effect of water soluble metalloporphyrins on Aβ1–42 aggregation, *Inorg. Chem. Front.*, 2022, **9**(7), 1520–1532.

65 V. Kovalska, S. Chernii, M. Losytskyy, J. Ostapko, I. Tretyakova, A. Gorski, V. Chernii and S. Yarmoluk, Activity of Zn and Mg phthalocyanines and porphyrazines in amyloid aggregation of insulin, *J. Mol. Recognit.*, 2018, **31**(1), e2660.

66 S. K. Shoffner and S. Schnell, Estimation of the lag time in a subsequent monomer addition model for fibril elongation, *Phys. Chem. Chem. Phys.*, 2016, **18**(31), 21259–21268.

67 E. Stefaniak, E. Atrian-Blasco, W. Goch, L. Sabater, C. Hureau and W. Bal, The Aggregation Pattern of Aβ1–40 is Altered by the Presence of N-Truncated Aβ4–40 and/or CuII in a Similar Way through Ionic Interactions, *Chem. – Eur. J.*, 2021, **27**(8), 2798–2809.

68 Y. Tian and J. H. Viles, pH Dependence of Amyloid-β Fibril Assembly Kinetics: Unravelling the Microscopic Molecular Processes, *Angew. Chem., Int. Ed.*, 2022, **61**(48), e202210675.

69 R. T. Wheelhouse, D. Sun, H. Han, F. X. Han and L. H. Hurley, Cationic Porphyrins as Telomerase Inhibitors: the Interaction of Tetra-(N-methyl-4-pyridyl) porphine with Quadruplex DNA, *J. Am. Chem. Soc.*, 1998, **120**(13), 3261–3262.

70 J. M. Kelly, M. J. Murphy, D. J. McConnell and C. OhUigin, A comparative study of the interaction of 5,10,15,20-tetrakis (N-methylpyridinium-4-yl)porphyrin and its zinc complex with DNA using fluorescence spectroscopy and topoisomerisation, *Nucleic Acids Res.*, 1985, **13**(1), 167–184.

71 R. Teixeira, V. V. Serra, D. Botequim, P. M. R. Paulo, S. M. Andrade and S. M. B. Costa, Fluorescence Spectroscopy of Porphyrins and Phthalocyanines: Some Insights into Supramolecular Self-Assembly, Microencapsulation, and Imaging Microscopy, *Molecules*, 2021, **26**(14), 4264.

72 J. Bohandy and B. F. Kim, in *Spectroscopy of Porphyrins*, ed. J. H. A. T. Digest, 1981.

73 S. Zakavi and S. Hoseini, The absorption and fluorescence emission spectra of meso-tetra(aryl)porphyrin dications with weak and strong carboxylic acids: a comparative study, *RSC Adv.*, 2015, **5**(129), 106774–106786.

74 S. Vivekanandan, J. R. Brender, S. Y. Lee and A. Ramamoorthy, A partially folded structure of amyloid-beta(1–40) in an aqueous environment, *Biochem. Biophys. Res. Commun.*, 2011, **411**(2), 312–316.

75 J. Danielsson, R. Pierattelli, L. Banci and A. Graslund, High-resolution NMR studies of the zinc-binding site of the Alzheimer's amyloid beta-peptide, *FEBS J.*, 2007, **274**(1), 46–59.

76 L. Hou, H. Shao, Y. Zhang, H. Li, N. K. Menon, E. B. Neuhaus, J. M. Brewer, I. J. Byeon, D. G. Ray, M. P. Vitek, T. Iwashita, R. A. Makula, A. B. Przybyla and M. G. Zagorski, Solution NMR studies of the A beta(1–40) and A beta(1–42) peptides establish that the Met35 oxidation state affects the mechanism of amyloid formation, *J. Am. Chem. Soc.*, 2004, **126**(7), 1992–2005.

77 A. Wahlström, R. Cukalevski, J. Danielsson, J. Jarvet, H. Onagi, J. Rebek Jr, S. Linse and A. Gräslund, Specific Binding of a β-Cyclodextrin Dimer to the Amyloid β Peptide Modulates the Peptide Aggregation Process, *Biochemistry*, 2012, **51**(21), 4280–4289.

78 C. Wallin, J. Jarvet, H. Biverstål, S. Wärmländer, J. Danielsson, A. Gräslund and A. Abelein, Metal ion coordination delays amyloid-β peptide self-assembly by forming an aggregation–inert complex, *J. Biol. Chem.*, 2020, **295**(21), 7224–7234.

79 B. N. Briggs, A. J. Gaier, P. E. Fanwick, D. K. Dogutan and D. R. McMillin, Cationic Copper(II) Porphyrins Intercalate into Domains of Double-Stranded RNA, *Biochemistry*, 2012, **51**(38), 7496–7505.

80 J. Li, Y. Wei, L. Guo, C. Zhang, Y. Jiao, S. Shuang and C. Dong, Study on spectroscopic characterization of Cu porphyrin/Co porphyrin and their interactions with ctDNA, *Talanta*, 2008, **76**(1), 34–39.

81 K. M. Kadish, K. M. Smith and R. Guilard, *The porphyrin handbook. Inorganic, organometallic and coordination chemistry*, Academic San Diego, Calif, San Diego, Calif, 2000, vol. 3.

82 E. B. Fleischer, Structure of porphyrins and metalloporphyrins, *Acc. Chem. Res.*, 1970, **3**(3), 105–112.

83 F. H. Köhler, Paramagnetic Complexes in Solution: The NMR Approach, in *eMagRes*, ed. R. K. Harris and

R. L. Wasylishen, Wiley, 2011, DOI: 10.1002/9780470034590.emrstm1229.

84 C. Hureau and P. Dorlet, Coordination of redox active metal ions to the APP protein and to the amyloid-β peptides involved in Alzheimer disease. Part 2: How Cu(II) binding sites depend on changes in the Aβ sequences, *Coord. Chem. Rev.*, 2012, **256**(19–20), 2175–2187.

85 J. Jumper, R. Evans, A. Pritzel, T. Green, M. Figurnov, O. Ronneberger, K. Tunyasuvunakool, R. Bates, A. Žídek, A. Potapenko, A. Bridgland, C. Meyer, S. A. A. Kohl, A. J. Ballard, A. Cowie, B. Romera-Paredes, S. Nikolov, R. Jain, J. Adler, T. Back, S. Petersen, D. Reiman, E. Clancy, M. Zielinski, M. Steinegger, M. Pacholska, T. Berghammer, S. Bodenstein, D. Silver, O. Vinyals, A. W. Senior, K. Kavukcuoglu, P. Kohli and D. Hassabis, Highly accurate protein structure prediction with AlphaFold, *Nature*, 2021, **596**(7873), 583–589.

86 M. Biancalana and S. Koide, Molecular mechanism of Thioflavin-T binding to amyloid fibrils, *Biochim. Biophys. Acta, Proteins Proteomics*, 2010, **1804**(7), 1405–1412.

87 A. A. Reinke and J. E. Gestwicki, Insight into Amyloid Structure Using Chemical Probes, *Chem. Biol. Drug Des.*, 2011, **77**(6), 399–411.

88 R. Sabaté and S. Ventura, Cross-β-Sheet Supersecondary Structure in Amyloid Folds: Techniques for Detection and Characterization, in *Protein Supersecondary Structures*, ed. A. E. Kister, Humana Press, Totowa, NJ, 2013, pp. 237–257.

89 R. Riek, The Three-Dimensional Structures of Amyloids, *Cold Spring Harbor Perspect. Biol.*, 2017, **9**(2), a023572.

90 S. Noël, S. Cadet, E. Gras and C. Hureau, The benzazole scaffold: a SWAT to combat Alzheimer's Disease, *Chem. Soc. Rev.*, 2013, **42**, 7747–7762.

91 A. I. Sulatskaya, G. N. Rychkov, M. I. Sulatsky, E. V. Mikhailova, N. M. Melnikova, V. S. Andozhskaya, I. M. Kuznetsova and K. K. Turoverov, New Evidence on a Distinction between Aβ40 and Aβ42 Amyloids: Thioflavin T Binding Modes, Clustering Tendency, Degradation Resistance, and Cross-Seeding, *Int. J. Mol. Sci.*, 2022, **23**(10), 5513.

92 M. Li, A. Zhao, J. Ren and X. Qu, N-Methyl, Mesoporphyrin IX as an Effective Probe for Monitoring Alzheimer's Disease β-Amyloid Aggregation in Living Cells, *ACS Chem. Neurosci.*, 2017, **8**(6), 1299–1304.

93 C. Yuan and Z. Gao, Aβ interacts with both the iron center and the porphyrin ring of heme: mechanism of heme's action on Aβ aggregation and disaggregation, *Chem. Res. Toxicol.*, 2013, **26**, 262.

94 B. R. Sahoo, T. Genjo, T. W. Nakayama, A. K. Stoddard, T. Ando, K. Yasuhara, C. A. Fierke and A. Ramamoorthy, A cationic polymethacrylate-copolymer acts as an agonist for β-amyloid and an antagonist for amylin fibrillation, *Chem. Sci.*, 2019, **10**(14), 3976–3986.

95 F. Liu, W. Zhao, F. Zhao, Q. Dong, Y. Wang, W. Wei, L. Jia, L. Li and F. Lu, Dual Effect of the Acidic Polysaccharose Ulvan on the Inhibition of Amyloid-β Protein Fibrillation and Disintegration of Mature Fibrils, *ACS Appl. Mater. Interfaces*, 2020, **12**(37), 41167–41176.

96 M. Ramesh, A. Acharya, N. A. Murugan, H. Ila and T. Govindaraju, Thiophene-Based Dual Modulators of Aβ and Tau Aggregation, *ChemBioChem*, 2021, **22**(23), 3348–3357.

97 D. Pramanik, C. Ghosh and S. G. Dey, Heme–Cu Bound Aβ Peptides: Spectroscopic Characterization, Reactivity, and Relevance to Alzheimer's Disease, *J. Am. Chem. Soc.*, 2011, **133**(39), 15545–15552.

98 G. Thiabaud, S. Pizzocaro, R. Garcia-Serres, J.-M. Latour, E. Monzani and L. Casella, Heme Binding Induces Dimerization and Nitration of Truncated β-Amyloid Peptide Aβ16 Under Oxidative Stress, *Angew. Chem., Int. Ed.*, 2013, **52**(31), 8041–8044.

99 C. Bacchella, J. T. Brewster, S. Bähring, S. Dell'Acqua, H. D. Root, G. D. Thiabaud, J. F. Reuther, E. Monzani, J. L. Sessler and L. Casella, Condition-Dependent Coordination and Peroxidase Activity of Hemin-Aβ Complexes, *Molecules*, 2020, **25**(21), 5044.

100 J. Gout, F. Meuris, A. Desbois and P. Dorlet, In vitro coordination of Fe-protoheme with amyloid beta is non-specific and exhibits multiple equilibria, *J. Inorg. Biochem.*, 2022, **227**, 111664.